Four Intercomponent Processes in a Ru(II)-Rh(III) Polypyridine Dyad: Electron Transfer from Excited Donor, Electron Transfer to Excited Acceptor, Charge Recombination, and Electronic Energy Transfer

M. T. Indelli,*,† C. A. Bignozzi,† A. Harriman,‡ J. R. Schoonover,§,∥ and F. Scandola*,†

Contribution from the Dipartimento di Chimica dell'Università, Centro di Fotoreattività e Catalisi CNR, 44100 Ferrara, Italy, the Center for Fast Kinetics Research, The University of Texas at Austin, Austin, Texas 78712, and the Chemistry Department, The University of North Carolina, Chapel Hill, North Carolina 27599-3290

Received November 5, 1993®

Abstract: The binuclear complex $Ru^{II}(Me_2phen)_2$-(Mebpy-CH_2-CH_2-Mebpy)-$Rh^{III}(Me_2bpy)_2^{5+}$ (Me_2phen = 4,7-dimethyl-1,10-phenanthroline; Mebpy = 4-methyl-2,2′-bipyridine; Me_2bpy = 4,4′-dimethyl-2,2′-bipyridine), hereafter represented by Ru(II)-Rh(III), was synthesized and studied. Selective excitation of the two moieties of the dyad was achieved with visible (100% *Ru(II)-Rh(III)) or ultraviolet light (e.g., at 298 nm, 70% Ru(II)-*Rh(III)). In room-temperature fluid solutions, both local excited states are quenched by electron transfer, leading to a common Ru(III)-Rh(II) state. The two forward electron-transfer processes, as well as the recombination process leading back to the ground state, can be resolved by transient laser spectroscopy, using various excitation wavelengths and pulse widths (532 nm, 30 ps; 427 nm, 0.5 ps; 298 nm, 0.5 ps). Rate constants in acetonitrile are as follows: *Ru(II)-Rh(III) → Ru(III)-Rh(II), 1.7×10^8 s^{-1}; Ru(II)-*Rh(III) → Ru(III)-Rh(II), 3.3×10^{10} s^{-1}; Ru(III)-Rh(II) → Ru(II)-Rh(III), 7.1×10^9 s^{-1}. The rate constants can be rationalized in terms of standard electron-transfer theory, assuming that the driving force ($\Delta G°$ = -0.10, -0.70, and -2.07 eV, respectively) is the main variable parameter. The two forward processes belong to the "normal", and the back reaction belongs to the "inverted" free-energy regime. In room-temperature fluid solution, no Ru(II)-*Rh(III) → *Ru(II)-Rh(III) energy transfer ($\Delta G°$ = -0.61 eV) is observed, presumably because of efficient competition by the faster Ru(II)-*Rh(III) → Ru(III)-Rh(II) electron-transfer quenching. By contrast, this process becomes efficient in rigid media (room-temperature or 77 K), where both the *Ru(II)-Rh(III) → Ru(III)-Rh(II) and Ru(II)-*Rh(III) → Ru(III)-Rh(II) electron-transfer processes are blocked as a consequence of restricted solvent repolarization. In 77 K ethanol glass, the energy-transfer rate constant is 1.9×10^6 s^{-1}.

Introduction

The study of photoinduced electron transfer in covalently linked donor-acceptor systems ("dyads")[1-12] has been of great value in several respects. From a fundamental standpoint, it has greatly contributed to shape our present understanding of electron-transfer processes. On the other hand, it has opened the way toward artificial photosynthetic centers, i.e., more complex systems (triads, tetrads, and pentads) where multiple electron-transfer steps lead to fast charge separation over long intercomponent distances.[13]

Typically, a dyad consists of two molecular components with distinct properties and roles: (i) a photoexcitable group ("chromophore") with a long-lived excited state and appropriate excited-state redox properties; (ii) a nonchromophoric component ("quencher") with appropriate ground-state redox properties. Among the large number of organic and inorganic dyads studied so far, the most common situation is that shown in Figure 1a, where the chromophore acts as an excited-state electron donor (D) and the quencher as an electron acceptor (A). Usually, the rate of the forward electron transfer step (process cs, often called "charge separation") can be determined easily by comparison between the excited-state properties of the chromophore in the dyad and as a free molecule. In favorable cases, the rate of the back electron transfer process (process cr, usually called "charge recombination") can be monitored by transient absorption spectroscopy.

In this article, we would like to describe the behavior of a peculiar type of dyad (Figure 1b), in which both the electron donor and the electron acceptor are photoexcitable (chromophoric) units. This permits the observation, in a single dyad, of several intercomponent transfer processes, namely, (i) electron transfer from excited donor to acceptor (process cs), (ii) electron transfer from donor to excited acceptor (process cs′), (iii) back electron transfer from reduced acceptor to oxidized donor (process cr),

† University of Ferrara.
‡ The University of Texas at Austin.
§ University of North Carolina.
∥ Present address: Los Alamos National Laboratories, Los Alamos, NM 87545.

® Abstract published in *Advance ACS Abstracts,* March 15, 1994.

(1) Joran, A. D.; Leland, B. A.; Felker, P. M.; Zewail, A. H.; Hopfield, J. J.; Dervan, P. B. *Nature* **1987**, *327*, 508.
(2) Closs, G. L.; Miller, J. R. *Science* **1988**, *240*, 440.
(3) Wasielewski, M. R. In *Photoinduced Electron Transfer*; Fox, M. A., Chanon, M., Eds.; Elsevier: Amsterdam, The Netherlands, 1988; Part A, p 161.
(4) Connolly, J. S.; Bolton, J. R. In *Photoinduced Electron Transfer*; Fox, M. A., Chanon, M., Eds.; Elsevier: Amsterdam, The Netherlands, 1988; Part D, p 303.
(5) Finckh, P.; Heitele, H.; Volk, M.; Michel-Beyerle, M. E. *J. Phys. Chem.* **1988**, *92*, 6584.
(6) Balzani, V.; Scandola, F. *Supramolecular Photochemistry*; Horwood: Chichester, U. K., 1991; Chapter 5.
(7) Verhoeven, J. W.; Paddon-Row, M. N.; Warman, J. M. In *Photoprocesses in Transition Metal Complexes, Biosystems and Other Molecules. Experiments and Theory*; Kochanski, E., Ed.; Kluwer: Dordrecht, The Netherlands, 1992.
(8) MacQueen, D. B.; Schanze, K. S. *J. Am. Chem. Soc.* **1991**, *113*, 7470.
(9) Ryu, C. K.; Wang, R.; Schmehl, R. H.; Ferrere, S.; Ludwikow, M.; Merkert, J. W.; Headford, C. E. L.; Elliott, C. M. *J. Am. Chem. Soc.* **1992**, *114*, 430.
(10) Collin, J. P.; Guillerez, S.; Sauvage, J.-P.; Barigelletti, F.; De Cola, L.; Flamigni, L.; Balzani, V. *Inorg. Chem.* **1992**, *31*, 4112.
(11) Meckenburg, S. L.; Peek, B. M.; Erickson, B. W.; Meyer, T. J. *J. Am. Chem. Soc.* **1991**, *113*, 8540.
(12) De Cola, L.; Balzani, V.; Barigelletti, F.; Flamigni, L.; Belser, P.; von Zelewsky, A.; Frank, M.; Vögtle, F. *Inorg. Chem.* **1993**, *32*, 5228. Vögtle, F.; Frank, M.; Nieger, M.; Belser, P.; von Zelewsky, A.; Balzani, V.; Barigelletti, F.; De Cola, L.; Flamigni, L. *Angew. Chem., Int. Ed. Engl.* **1993**, *32*, 1643.
(13) Moore, T. A.; Gust, D.; Moore, A. L. In *Supramolecular Chemistry*; Balzani, V., De Cola, L., Eds.; Kluwer: Dordrecht, The Netherlands, 1992; p 295.

0002-7863/94/1516-3768$04.50/0

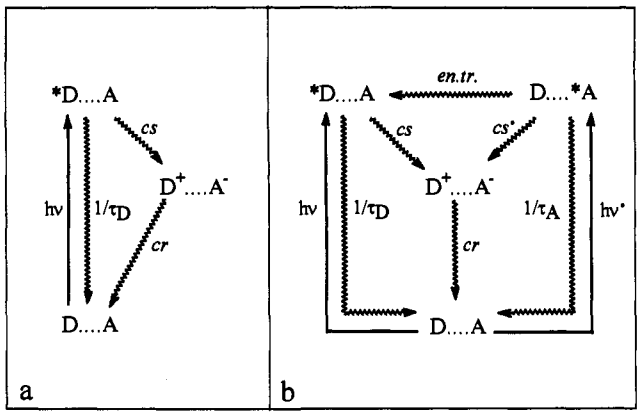

Figure 1. Intercomponent processes taking place in (a) a typical donor-acceptor dyad of the chromophore-quencher type and (b) a dyad allowing excitation of *both* electron donor and electron acceptor (see text).

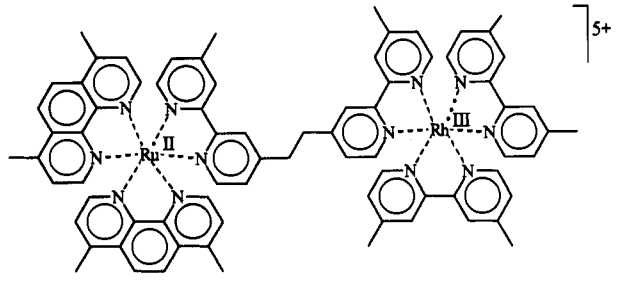

Figure 2. Structural formula of the Ru(II)–Rh(III) dyad.

and (iv) energy transfer from excited acceptor to the donor (process en.tr.; notice that in such a scheme the *electron* acceptor is the *energy* donor, and vice versa).

The dyad $Ru^{II}(Me_2phen)_2$–(Mebpy–CH_2–CH_2–Mebpy)–$Rh^{III}(Me_2bpy)_2^{5+}$ (Me_2phen = 4,7-dimethyl-1,10-phenanthroline; Mebpy = 4-methyl-2,2′-bipyridine; Me_2bpy = 4,4′-dimethyl-2,2′-bipyridine), hereafter referred to as Ru(II)–Rh(III), is schematically represented in Figure 2. It consists of two structurally similar inorganic components, namely, metal tris(polypyridine) complexes, linked by an ethylene chain. The electron donor or acceptor character of the components is determined by the metal center; the Ru(II) polypyridine unit acts as the donor (D in Figure 1b), and the Rh(III) polypyridine unit, as the acceptor (A in Figure 1b).[14]

Work on other Ru(II)–Rh(III) polypridine dyads, involving various ligands and bridging groups, has recently been reported.[15-17] In such studies, quenching of the Ru(II)-based emission in the dyad was observed, and such quenching was ascribed on a purely intuitive basis to intramolecular electron transfer. A study on a related Ru(II)–Co(III) dyad, in which again electron-transfer quenching is observed, has very recently appeared.[18] Mononuclear chromophore–quencher complexes of the Ru(II)–diquat[9,19] and Rh(III)–diquat[20] type can also be considered as related systems, as they involve the same double-bipyridine ligand (in which, however, the uncoordinated moiety is quaternarized so as to act as an electron acceptor).

Experimental Section

Materials. $(NH_4)_3RhCl_6$, $RuCl_3 \cdot 3H_2O$, 4,4′-dimethyl-2,2′-bipyridine (Me_2bpy), 4,7-dimethyl-1,10-phenanthroline (Me_2phen), and tetrabutylammonium hexafluorophosphate [TBA]PF_6 were purchased from Fluka. All the other chemicals were commercial products of reagent grade. $Ru(Me_2phen)_2Cl_2$,[21] $[Ru(Me_2phen)_3](PF_6)_2$,[22] $[Ru(Me_2bpy)_3](PF_6)_2$,[22] and $[Rh(Me_2bpy)_2Cl_2]Cl$[23] were prepared according to literature procedures. Sephadex CM-C25 (Pharmacia) was used in ionic exchange chromatography.

1,2-Bis[4-(4′-methyl-2,2′-bipyridinyl)]ethane (Mebpy–CH_2–CH_2–Mebpy). This ligand was prepared by the method described by Elliott and co-workers.[24]

$[Rh(Me_2bpy)_2$(Mebpy–CH_2–CH_2–Mebpy)$](ClO_4)_3$. A 0.28-g amount of $[Rh(Me_2bpy)_2Cl_2]Cl$ (0.48 mmol) was added to 50 mL of a hot 40/60 ethylene glycol/ethanol solution containing 0.7 g (1.9 mmol) of Mebpy–CH_2–CH_2–Mebpy. To the boiling solution was slowly added 25 mL of water. The solution was refluxed for 64 h. After evaporation of the EtOH, the reaction mixture was cooled to room temperature, diluted to 200 mL with water, and filtered to remove the excess Mebpy–CH_2–CH_2–Mebpy. The solution was loaded on a CM-C25 Sephadex column in Na^+ form. Some unreacted $[Rh(Me_2bpy)_2Cl_2]^+$ was first eluted with 0.05 M NaCl; then the product was collected with 0.2 M NaCl as eluant. The solution was concentrated, and the colorless perchlorate salt was precipitated by addition of concentrated $HClO_4$ and filtered. The product was washed with small portions of cold water and air-dried. Anal. Calcd for $[Rh(Me_2bpy)_2(Mebpy–CH_2–CH_2–Mebpy)(ClO_4)_3 \cdot H_2O$: C, 49.95; H, 4.19; N, 9.71. Found: C, 49.03; H, 4.13; N, 9.52.

$[Ru(Me_2phen)_2$(Mebpy–CH_2–CH_2–Mebpy)$](PF_6)_2$. A 0.2-g (0.35 mmol) amount of $Ru(Me_2phen)_2Cl_2$ was added to 50 mL of warm MeOH containing 0.4 g (1.09 mmol) of Mebpy–CH_2–CH_2–Mebpy. The solution was refluxed for 1.5 h and then evaporated to dryness. The residue was dissolved in water, the resulting solution was filtered to remove unreacted Mebpy-CH_2–CH_2–Mebpy and taken to dryness by rotary evaporation under vacuum. The product was purified by Al_2O_3 column chromatography, eluting with MeOH. The hexafluorophosphate salt was obtained by adding NH_4PF_6 to an aqueous solution of the product. Anal. Calcd for $[Ru(Me_2phen)_2(Mebpy–CH_2–CH_2–Mebpy)](PF_6)_2$: C, 53.20; H, 3.95; N, 9.54. Found: C, 52.82; H, 3.94; N. 9.38. Solutions of the oxidized form of this complex were prepared by oxidation with $(NH_4)_2Ce(NO_3)_6$ in acidic aqueous solution.

$[Ru(Me_2phen)_2$–(Mebpy–CH_2–CH_2–Mebpy)–$Rh(Me_2bpy)_2](PF_6)_5$. A 0.150-g (0.13 mmol) amount of $[Rh(Me_2bpy)_2(Mebpy–CH_2–CH_2–Mebpy)](ClO_4)_3$ and 0.040 g of $Ru(Me_2phen)_2Cl_2$ was refluxed in 10 mL of MeOH for 30 h under argon. After removal of the solvent, the residue was dissolved in a 1/1 H_2O/acetone solution and $NaClO_4$ was added. The product was precipitated by evaporation of acetone, filtered, dried under vacuum, and converted to the chloride salt by addition of tetrabutylammonium chloride to an acetonitrile solution of the perchlorate salt. The product was then purified by cationic exchange chromatography on Sephadex CM-C25 in H^+ form. Elution was first performed with 0.02 M HCl to remove the unreacted $[Rh(Me_2bpy)_2(Mebpy–CH_2–CH_2–Mebpy)]^{3+}$ and then with 0.05 M HCl to elute the product. The eluted solution was concentrated and the product precipitated by addition of NH_4PF_6. The complex was characterized by FAB mass spectrometry. In the FAB spectrum, the peak of highest m/z ratio was found at 1935. This corresponds to the value expected for a species originating from the salt examined by loss of one counterion (i.e., $[Ru(Me_2phen)_2$–(Mebpy–CH_2–CH_2–Mebpy)–$Rh(Me_2bpy)_2](PF_6)_4^+$), a feature common to other polynuclear complex salts.[25] Anal. Calcd for $[Ru(Me_2phen)_2$–(Mebpy–CH_2–CH_2–Mebpy)–$Rh(Me_2bpy)_2](PF_6)_5 \cdot 2H_2O$: C, 43.25; H, 3.53; N, 7.94. Found: C, 42.47; H, 3.48; N, 7.78.

Apparatus and Procedures. UV–vis spectra were recorded with a Kontron Uvikon 860 spectrophotometer. Emission and excitation spectra were taken on a Perkin Elmer MPF 44E spectrofluorimeter equipped

(14) Notice that in this case the usual labeling of "charge separation" for the forward electron transfer and "charge recombination" for the back electron transfer processes, originally coined for organic dyads, is not appropriate. In fact, due to the 2+ and 3+ charges on the two molecular components, both types of processes are examples of "charge exchange".

(15) Furue, M.; Hirata, M.; Kinoshita, S.; Kushida, T.; Kamachi, M. *Chem. Lett.* **1990**, 2065.
(16) Nozaki, K.; Ohno, T.; Haga, M. *J. Phys. Chem.* **1992**, *96*, 10880.
(17) Kalyanasundaram, K.; Graetzel, M.; Nazeeruddin, M. K. *J. Phys. Chem.* **1992**, *96*, 5865.
(18) Song, X.; Lei, Y.; Van Wallendal, S.; Perkovic, M. W.; Jackman, D. C.; Endicott, J. F.; Rillema, D. P. *J. Phys. Chem.* **1993**, *97*, 3225.
(19) Cooley, L. F.; Headford, C. E. L.; Elliott, C. M.; Kelley, D. F. *J. Am. Chem. Soc.* **1988**, *110*, 6673.
(20) Indelli, M. T.; Polo, E.; Bignozzi, C. A.; Scandola, F. *J. Phys. Chem.* **1991**, *95*, 3889.
(21) Sullivan, B. P.; Salomon, D. J.; Meyer, T. J. *Inorg. Chem.* **1978**, *17*, 3334.
(22) Mabrouk, P. A.; Wrighton, M. S. *Inorg. Chem.* **1986**, *25*, 526.
(23) Gillard, R. D.; Osborn, J. A.; Wilkinson, G. *J. Chem. Soc.* **1965**, 1951.
(24) Elliott, C. M.; Freitag, R. A.; Blaney, D. D. *J. Am. Chem. Soc.* **1985**, *107*, 4647.
(25) Argazzi, R.; Bignozzi, C. A.; Bortolini, O.; Traldi, P. *Inorg. Chem.* **1993**, *32*, 1222.

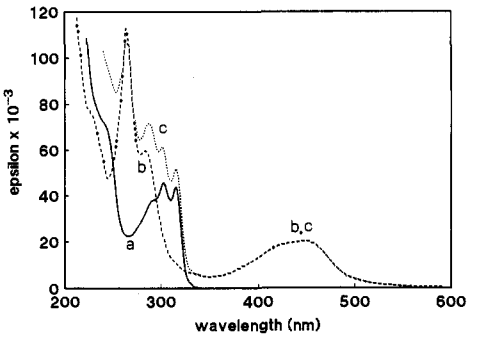

Figure 3. Absorption spectra of (a) $Rh(Me_2bpy)_2(Mebpy–CH_2–CH_2–Mebpy)^{3+}$, (b) $Ru(Me_2phen)_2(Mebpy–CH_2–CH_2–Mebpy)^{2+}$ and (c) the Ru(II)–Rh(III) dyad, in acetonitrile solution.

with a Hamamatsu R928 tube. The emission spectra were corrected for instrumental response by calibration with an NBS standard quartz–halogen lamp. Emission quantum yield values were obtained by using $Ru(bpy)_3^{2+}$ in water ($\Phi = 0.042$) as a reference emitter.

Emission lifetimes were measured by time-correlated, single-photon counting by using a PRA 3000 nanosecond fluorescence spectrometer equipped with a Model 510B nanosecond pulsed lamp and a Model 1551 cooled photomultiplier; the data were collected on a Tracor Northern multichannel analyzer and processed on a PDP11/03 computer using original PRA software. All measurements were carried out on deaerated solutions.

Transient absorption measurements were made with a variety of laser excitation sources. Conventional nanosecond laser flash photolysis experiments were made with a frequency-doubled Quantel YG480 Nd:YAG laser (pulse width 10 ns, maximum pulse energy 120 mJ). Output from the laser was either frequency-doubled to 266 nm (12 mJ per pulse) or used to pump a Rhodamine 610 dye laser. Output from the dye laser was frequency-doubled to give 8 mJ pulses at 305 nm. For all kinetic studies, the monitoring beam was provided by a pulsed xenon arc lamp and detection was made with a high radiance monochromator equipped with an R928 photomultiplier tube. Approximately 50 individual laser shots were averaged for each decay profile and data analysis was made by nonlinear least-squares iteration using a 386 microcomputer. Spectral measurements were made with a high-intensity pulsed (5 μs) xenon lamp which was sequenced to fire at a predetermined time with respect to laser excitation. Spectra were acquired with a Princeton dual diode array spectrograph. Low-temperature studies were made with the sample cell housed in a quartz Dewar filled with liquid nitrogen. All measurements were made after purging the solution with oxygen-free nitrogen.

Improved time resolution was achieved using a mode-locked, frequency-doubled Quantel YG402 Nd:YAG laser (pulse width 30 ps, maximum pulse energy 25 mJ). Part of the laser output was focused into a 1/1 mixture of D_2O/D_3PO_4 to produce a white light continuum for use as the monitoring pulse. The excitation pulse was delayed relative to the monitoring pulse using an optical delay stage, and the two pulses were directed almost collinearly through the sample cell. For each delay time, 300 individual laser shots were accumulated and averaged in the microcomputer. Kinetic profiles were constructed by overlaying spectra collected at about 30 different delay times. A Princeton dual diode array spectrograph was used as detector, and the time resolution of this instrument, after deconvolution of the instrumental response, was around 20 ps. The temporal window ranges from 20 ps to 7 ns, and for longer time scales a conventional optical bench fitted with a pulsed xenon arc lamp was used in place of the continuum generation setup.

Additional studies were made with a frequency-doubled Antares 76S mode-locked Nd:YAG-pumped Rhodamine 6G or Styryl-9 dye laser.[26] A Quantel Model RGA67-10 regenerative amplifier, operated at 10 Hz, and a Quantel Model PTA-60 dye laser were used to generate pulses at 596 nm (Rhodamine 6G) or 854 nm (Styryl-9) having a fwhm of about 500 fs. The output beam was split, as for the above picosecond experiments, and part was used to generate a white light continuum for use as the monitoring pulse. The excitation pulse was frequency-doubled to produce pulses at 298 nm (1 mJ) or 427 nm (0.3 mJ). Transient absorption spectral changes were determined by computer subtraction of sample and reference beams averaged over 600 individual laser shots using a Princeton dual diode array spectrograph. Decay kinetics were established by overlaying spectra collected at different delay times. The temporal window for this instruments ranges from 500 fs to 600 ps.

Raman spectra were measured at the University of North Carolina Laser Facility on previously described instrumentation.[27] The transient resonance Raman experiments were single-color experiments, performed with 354-nm laser pulses of halfwidth 7–10 ns. The intensity of the pulse was always sufficient to saturate the excited state, so that the first part of the pulse was used to excite the sample and the remaining part was used as a source of Raman scattering. The signal was integrated over a gate period of 50–100 ns, centered wide over the laser pulse. Given these features, it is impossible to give a precise definition of the "time resolution" of this technique. In practical terms, (i) excited states accessible to this technique must have lifetimes of 20 ns or longer, and (ii) the experimental spectrum can be considered as an average of the true excited-state resonance Raman spectra over the time range $t = 0$–20 ns.

Cyclic voltammetry measurements were carried out on Ar-purged CH_3CN solutions containing 0.1 M $[TBA]PF_6$ by using a previously described apparatus[28] and a conventional three-electrode cell (platinum, working; saturated calomel electrode (SCE), reference).

Table 1. Raman Frequencies (600–1700 cm^{-1}) for the Ground-State (CW, 457.9 nm) and Excited-State (Pulsed, 354.7 nm) Resonance Raman Spectra for $Ru(Me_2phen)_3^{2+}$ and $Ru(Me_2phen)_2(Mebpy–CH_2–CH_2–Mebpy)^{2+}$ (Abbreviated as RuP_3^{2+} and RuP_2B^{2+}, Respectively)

RuP_3^{2+}		RuP_2B^{2+}		
CW 457.9 nm	pulsed 354.7 nm	CW 457.9 nm	pulsed 354.7 nm	origin[a]
650		650		P
			725	B*
		741		B
		753		B
			788	B*
881	880	880	880	P
			1010	B*
1029		1029	1029	P, B
1123		1124		P
1177		1178		P
			1190	B*
1201		1201		P
			1210	B*
1243		1243		P
		1275		B
1288		1288	1288[b]	P
			1291	B*
1301		1301		P
	1303			P*
		1324		B
			1333	B*
	1338			P*
1347	1350[b]	1347	1350[b]	P
1410		1410	1410	P
	1415			P*
1445		1445		P
			1449	B*
	1452			P*
		1485		B
			1497	B*
			1503	B*
1519		1519	1519[b]	P
	1522			P*
		1549		B
	1560			P*
			1568	B*
1575		1575		P
	1581			P*
1605	1606	1605	1606	P
		1620		B
1620	1627	1628	1627	P

[a] P and B indicate ground-state Raman peaks originating from the respective ligands, while P* and B* indicate excited-state peaks (i.e., peaks originating from the formally reduced P and B ligands in Ru → P and Ru → B MLCT excited states). [b] Shoulder on a more intense peak.

(26) Atherton, S. J.; Harriman, A. *J. Am. Chem. Soc.* **1993**, *115*, 1816.

(27) Bignozzi, C. A.; Argazzi, R.; Chiorboli, C.; Scandola, F.; Dyer, R. B.; Schoonover, J. R.; Meyer, T. J. *Inorg. Chem.*, in press.

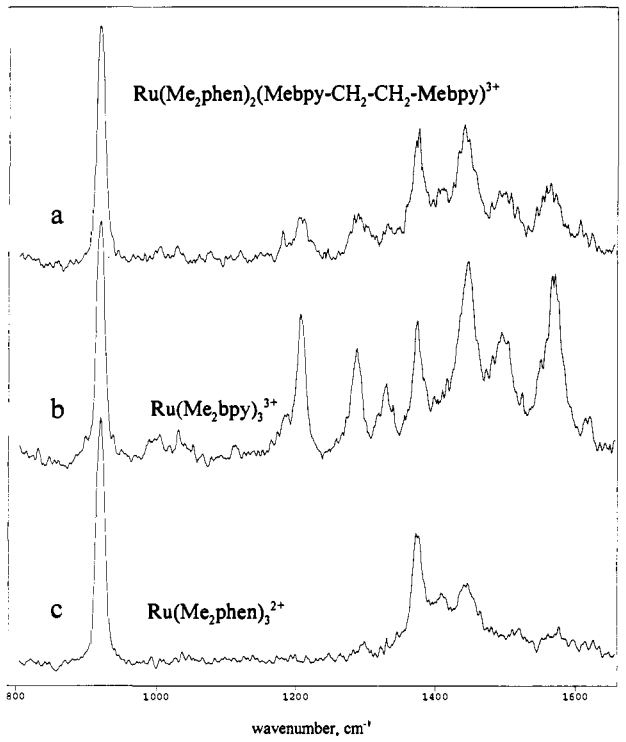

Figure 4. Time-resolved resonance Raman spectra of (a) $Ru(Me_2phen)_2(Mebpy–CH_2–CH_2–Mebpy)^{2+}$, (b) $Ru(Me_2bpy)_3^{2+}$, (c) $Ru(Me_2phen)_3^{2+}$ in acetonitrile solution. Spectra taken under appropriate conditions (optically matched solutions at the excitation wavelength) so as to provide meaningful relative scattering intensities.

Results

The spectroscopic, electrochemical, and photophysical properties of the Ru(II)–Rh(III) dyad can be compared with those of the mononuclear $Ru(Me_2phen)_2(Mebpy–CH_2–CH_2–Mebpy)^{2+}$ and $Rh(Me_2bpy)_2(Mebpy–CH_2–CH_2–Mebpy)^{3+}$ complexes that constitute the molecular models for the Ru(II) and Rh(III) components of the dyad, respectively.

UV–Vis Absorption Spectra. The absorption spectrum of the dyad is shown in Figure 3 together with the spectra of the Ru(II) and Rh(III) molecular models. As we can see from the figure, the absorption spectrum of the dyad is an exact superposition of the spectra of the isolated mononuclear species, with no new band being present. The Rh(III) component does not absorb in the visible region where the spectrum of the dyad is characterized by the typical metal-to-ligand charge transfer (MLCT) transitions of the Ru(II) component. In the UV region, both Ru(II) and Rh(III) components absorb; the bands centered at 280 and 295 nm correspond to ligand-centered (LC) transitions of the Ru(II) component, while those at 302 and 313 nm correspond to ligand-centered transitions of the Rh(III) component.

Resonance Raman Spectra. In an effort to obtain information on the localization of the lowest MLCT state on any particular ligand of the Ru(II)-based molecular component, transient resonance Raman spectra were measured for the following species: $Ru(Me_2phen)_2(Mebpy–CH_2–CH_2–bpyMe)^{2+}$ (as molecular model for the Ru(II) component in the dyad) and $Ru(Me_2phen)_3^{2+}$ and $Ru(Me_2bpy)_3^{2+}$ (as paradigmatic cases of Ru → Me_2phen and Ru → Me_2bpy excitations). The spectra were measured on 1.0×10^{-3} M acetonitrile solutions and are shown in Figure 4. In a separate experiment, the transient spectrum of a solution containing 0.67×10^{-3} M $Ru(Me_2phen)_3^{2+}$ and 0.33×10^{-3} M $Ru(Me_2bpy)_3^{2+}$ was also measured. This spectrum was indistinguishable from that of the 1.0×10^{-3} M solution of $Ru(Me_2phen)(Mebpy–CH_2–CH_2–bpyMe)^{2+}$ (Figure 4a). Frequencies and assignments for transient and ground-state resonance Raman spectra of $Ru(Me_2phen)_2(Mebpy–CH_2–CH_2–bpyMe)^{2+}$ and $Ru(Me_2phen)_3^{2+}$ are given in Table 1. The data for $Ru(Me_2bpy)_3^{2+}$ compare well to published data.[22] The strong bands observed in Figure 4 at 920 and 1372 cm^{-1} are due to the CH_3CN solvent.

Electrochemical Behavior. The electrochemical behavior of the Ru(II)–Rh(III) dyad was studied by cyclic voltammetry in CH_3CN solution ($[TBA]PF_6$ 0.1 M supporting electrolyte, Pt working electrode, SCE reference electrode). For purposes of comparison, the electrochemical behavior of the mononuclear $Ru(Me_2phen)_2(Mebpy–CH_2–CH_2–Mebpy)^{2+}$ and $Rh(Me_2bpy)_2(Mebpy–CH_2–CH_2–Mebpy)^{3+}$ complexes was studied under the same experimental conditions.

The cyclic voltammogram of the Ru(II) model is typical of Ru(II) polypyridine complexes.[29,30] A reversible oxidation wave, corresponding to oxidation of the Ru(II) center, is observed at +1.14 V. In the cathodic region (0, −1.9 V vs SCE), three reversible reduction waves corresponding to reduction of the three polypridine ligands were observed (Table 2). In contrast to the totally irreversible behavior in aqueous solution, the mononuclear $Rh(Me_2bpy)_2(Mebpy–CH_2–CH_2–Mebpy)^{3+}$ complex has been seen to exhibit quasireversible behavior in acetonitrile at rapid sweep rates.[30–32] At v = 0.02–0.05 V s^{-1} a reduction peak at −0.93 V vs SCE is observed. This reduction peak is accompanied by an anodic peak at −0.83 V if the scan direction is reversed rapidly (v = 0.5–1 V s^{-1}). From these results an $E_{1/2}$ value of −0.89 V vs SCE can be estimated (Table 2), in good agreement with the value reported by Creutz for the analogous $Rh(4,4'\text{-}Me_2bpy)_3^{3+}$ complex.[32]

The cyclic voltammogram of the dyad is practically the superposition of the corresponding curves of the $Ru(Me_2phen)_2(Mebpy–CH_2–CH_2–Mebpy)^{2+}$ and $Rh(Me_2bpy)_2(Mebpy–CH_2–CH_2–Mebpy)^{3+}$ model compounds. The electrochemical waves of the dyad, therefore, can be easily assigned by comparison with the waves observed for the isolated compounds (see Table 2).

Emission Measurements. The photophysical behavior was studied under comparable conditions for the model compounds and for the dyad.

The $Ru(Me_2phen)_2(Mebpy–CH_2–CH_2–Mebpy)^{2+}$ complex at room temperature exhibits the long-lived MLCT luminescence typical of Ru(II) polypyridine complexes[29,30] with a maximum at 610 nm in CH_3CN solution (Figure 5a). A quantum yield Φ = 0.11 and a lifetime τ = 1.8 μs were measured for this emission in deaerated acetonitrile at room temperature. In a rigid matrix (4/1 EtOH/MeOH) at 77 K, the emission becomes structured and shifts to the blue, with a maximum at 575 nm (Figure 4b). The lifetime at 77 K is 7 μs.

The photophysical behavior of $Rh(Me_2bpy)_2(Mebpy–CH_2–CH_2–Mebpy)^{3+}$ is typical of the Rh(III) tris(polypyridine) complexes.[30,33–36] In a rigid matrix (4/1 EtOH/MeOH) at 77 K, it exhibits an intense, highly structured ligand-centered (LC) phosphorescence in the 440–600-nm range with the high-energy band located at 448 nm. At room temperature the complex is practically nonemitting but the LC triplet can be detected by transient absorption. As for other Rh(III) polypyridine complexes,[20,36,37] however, an excited-state absorption (ESA) signal

(28) Bignozzi, C. A.; Roffia, S.; Chiorboli, C.; Davila, J.; Indelli, M. T.; Scandola, F. *Inorg. Chem.* **1989**, *28*, 4350.
(29) Juris, A.; Balzani, V.; Barigelletti, F.; Campagna, S.; Belser, P.; von Zelewsky, A. *Coord. Chem. Rev.* **1988**, *27*, 4587.
(30) Kalyanasundaram, K. *Photochemistry of Polypyridine and Porphyrin Complexes*, Academic: New York, 1992.
(31) Hanck, K.; DeArmond, K. *J. Phys. Chem.* **1975**, *79*, 1829.
(32) Creutz, C.; Keller, A. D.; Sutin, N.; Zipp, A. P. *J. Am. Chem. Soc.* **1982**, *104*, 3618.
(33) Carstens, D. H. W.; Crosby, G. A. *J. Mol. Spectrosc.* **1970**, *34*, 113.
(34) De Armond, M. K.; Hillis, J. E. *J. Chem. Phys.* **1971**, *54*, 2247.
(35) Watts, R. J.; Van Houten, J. *J. Am. Chem. Soc.* **1978**, *100*, 1718.
(36) Indelli, M. T.; Scandola, F. *Inorg. Chem.* **1990**, *29*, 3056.
(37) Indelli, M. T.; Carioli, A.; Scandola, F. *J. Phys. Chem.* **1984**, *88*, 2685.

Table 2. Half-Wave Potentials of the Ru(II)–Rh(III) Dyad and of the Model Compounds[a]

complex	redox process				
	Ru(III)/Ru(II)	Rh(III)/Rh(II)	L/L⁻(1)	L/L⁻(2)	L/L⁻(3)
$Ru(Me_2phen)_2(Mebpy–CH_2–CH_2–Mebpy)^{2+}$	+1.14		−1.45	−1.60	−1.82
$Rh(Me_2bpy)_2(Mebpy–CH_2–CH_2–Mebpy)^{3+}$		−0.89[b]			
Ru(II)–Rh(III)	+1.13	−0.92[b]	−1.45	−1.66	

[a] In CH_3CN solution, $[TBA]PF_6$ 0.1 M, Pt working electrode, vs SCE, values calculated as an average of the cathodic and anodic peaks. [b] ΔE_p = 100 mV.

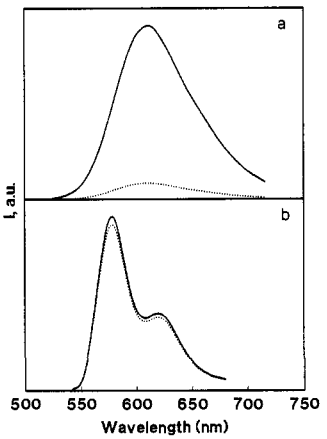

Figure 5. Emission spectra (a) at room temperature in acetonitrile solution, and (b) at 77 K in EtOH/MeOH 4/1 rigid matrix of $Ru(Me_2phen)_2(Mebpy–CH_2–CH_2–Mebpy)^{2+}$ (continuous line) and the Ru(II)–Rh(III) dyad (dotted line).

decaying in the nanosecond time scale can be used to monitor the excited state (see below).

As far as the photophysical behavior of the dyad is concerned, the important observation is that at room temperature in CH_3CN solution, upon excitation of the Ru(II) component, the typical MLCT emission of this unit is strongly quenched with respect to that of the free Ru(II) model (Figure 5a). The spectral profile of the residual Ru(II)-based emission is identical to that of the free Ru(II) complex. The comparison with the emission quantum yield (Φ_0 of the Ru(II) model (absorbance-matched solutions) gave a value for Φ_0/Φ of 90. The emission decay was clearly multiexponential. The experimental decay measured in deaerated CH_3CN solution at room temperature is shown in Figure 6. It consists of two components: a major (ca. 85%) short-lived component with a lifetime of 6 ns and a minor (ca. 15%) long-lived component with a lifetime of ≥30 ns. The excitation spectrum of the residual Ru(II)-based emission in room-temperature fluid CH_3CN solution is shown in Figure 7. It differs considerably in the ultraviolet range from the absorption spectrum of the dyad (Figure 3).

The emission properties of the Ru(II)–Rh(III) dyad were also studied in a ridid matrix at 77 K (4/1 EtOH/MeOH) as well as at room temperature in a poly(methyl methacrylate) (PMMA) matrix. At 77 K, the Ru(II)-based emission is not appreciably quenched (Figure 5b). The emission decay is strictly monoexponential with a lifetime of 6.8 μs, practically identical to that of the Ru(II) model. The excitation spectrum (Figure 7) matches very closely the absorption spectrum of the dyad (Figure 3). Very similar emission behavior (no quenching of the Ru(II)-based emission and a good match between absorption and excitation spectra) was observed in a rigid PMMA matrix at room temperature.

Transient Absorption Measurements. The behavior of the model compounds was straightforward. The transient absorption spectrum of the Ru(II) model compound (absorption at 365 nm and bleaching at 450 nm) is typical for this class of compounds.[30,38,39] At room temperature it decays with a lifetime of

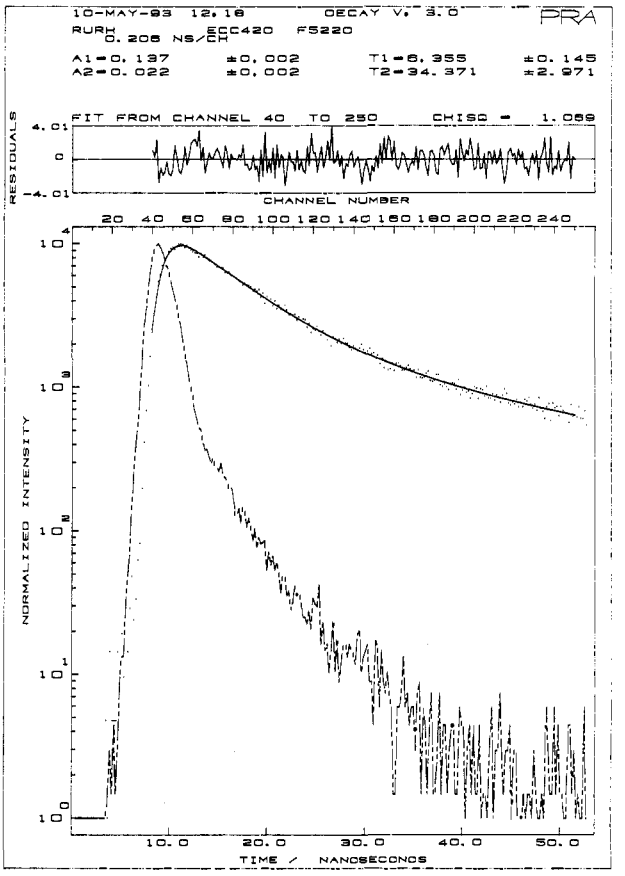

Figure 6. Emission decay of the Ru(II)–Rh(III) dyad in room temperature deaerated acetonitrile solution. Channel width, 0.206 ns/ch.

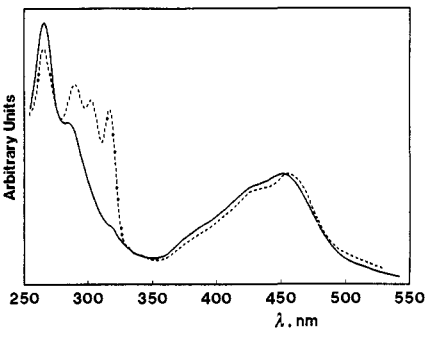

Figure 7. Excitation spectrum of the Ru(II)–Rh(III) dyad at room temperature in acetonitrile (continuous line) and at 77 K in EtOH/MeOH rigid matrix (broken line).

1.8 μs (deaerated acetonitrile), consistent with the emission lifetime. At 77 K in an ethanol glass the lifetime becomes 7.8 μs. The ESA of the Rh(III) model compound consists of a very weak spectrum centered at 390 nm. It decays with a lifetime of ca. 4.2 ns at 295 K (deaerated EtOH). At 77 K (ethanol glass) the lifetime becomes 2.4 ms.

(38) Braterman, P. S.; Harriman, A.; Heath, G. A.; Yellowless, L. *J. Chem. Soc., Dalton Trans.* **1983**, 1801.
(39) Watts, R. J. *J. Chem. Educ.* **1983**, *60*, 834.

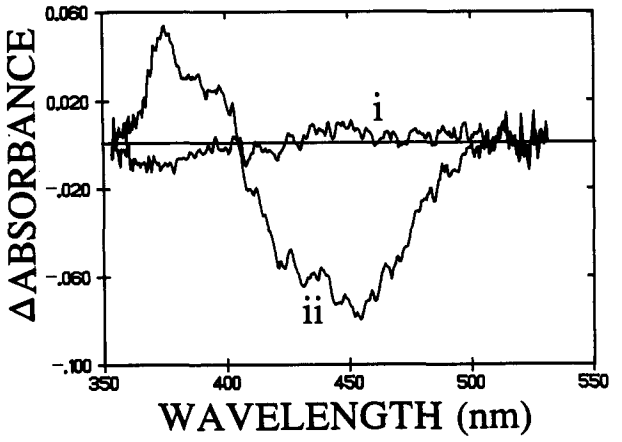

Figure 8. Transient absorption spectrum recorded (i) 5 ps before and (ii) 5 ps after excitation of the Ru(II)–Rh(III) dyad in deoxygenated acetonitrile at 295 K with a 0.5-ps laser pulse at 427 nm.

The behavior of the Ru(II)–Rh(III) dyad at room temperature was investigated using different excitation wavelengths and pulse widths: 0.5-ps pulses at 427 nm, 30-ps pulses at 532 nm, and 0.5-ps pulses at 298 nm. At 298 nm, a significant (ca. 70%) fraction of the incident light is absorbed (Figure 3) by the Rh(III) component. At 427 and 532 nm, light is selectively absorbed by the Ru(II) molecular component. It should be noted that the white light continuum generated with a 30-ps laser pulse is significantly less enriched in UV light than that generated from a 500-fs laser pulse. Thus, the continuum observed for the 30-ps pulse width experiments does not provide sufficient UV light to make measurements below about 390 nm whereas the continuum obtained in the 500-fs experiments allows measurements to be made at 370 nm. A different problem relates to the temporal windows that can be covered by the two instruments; whereas the 500-fs experiments can be made on time scales only up to about 600 ps, the 30-ps experiments can record spectra up to 7 ns and kinetic profiles up to the millisecond time scale. Since the triplet state of the ruthenium(II) chromophore shows an absorption band centered at 365 nm (and measurements at 390 nm are not really diagnostic of the triplet), it is necessary to use a variety of excitation sources in order to properly characterize transient decay for this system.

With a 0.5-ps excitation at 427 nm, the observed transient differential absorption spectrum (Figure 8) is indistinguishable from that recorded for the ruthenium(II) model and is assigned, therefore, to the localized MLCT triplet state. This species shows negligible decay on time scales up to 600 ps both at 370 and 450 nm. These observations indicate that the triplet state does not decay on such times scales. A similar, if not identical, transient absorption profile is observed following excitation with a 30-ps laser pulse at 532 nm (Figure 9a). In this case, there is partial deactivation of the transient over the accessible time window (<7 ns) and very good agreement between the kinetics for ground state recovery at 450 nm (Figure 9b) and triplet decay at 390 nm (Figure 9c). Because of the poor precision attained with picosecond laser flash photolysis techniques and the restricted time windows, accurate kinetic measurements are not possible for these particular studies. The kinetic profiles fit reasonably well to single-exponential decay laws, but following from the time-resolved luminescence studies described earlier, the profiles were compared with two-exponential decays laws. The fit to lifetimes of 6 ns (85%) and 40 ns (15%) are quite acceptable (Figure 9b and c).

The decay profiles for laser excitation with a 30-ps pulse at 532 nm were recorded on longer time scales using a fast photomultiplier tube (Figure 10) Again, the kinetics for decay of the triplet at 370 nm and recovery of the ground state at 450 nm are very similar and there was no spectral evidence to indicate

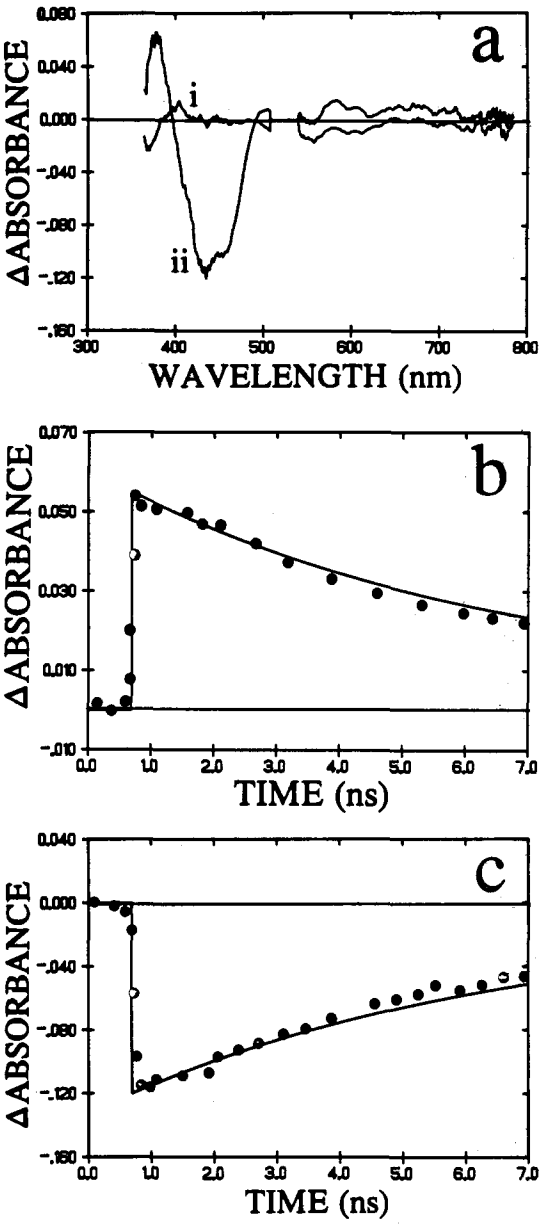

Figure 9. (a) Transient absorption spectrum recorded (i) 30 ps before, and (ii) 30 ps after excitation of the Ru(II)–Rh(III) dyad in deoxygenated acetonitrile at 295 K with a 30-ps laser pulse at 532 nm. (b) Kinetic profile for decay of the initial transient recorded at 390 nm for the above experiment. (c) Kinetic profile for recovery of the ground state at 450 nm in the same experiment. The solid lines drawn in traces b and c represent a fit of the data points to a two-exponential decay law with lifetimes of 6 ns (85%) and 40 ns (15%) (as suggested by time-resolved luminescence experiments).

intermediate formation of redox products. In this case, the decay profiles were analyzed by computer "best fit" procedures and the derived parameters corresponded to lifetimes of 5.3 ns (90%) and 28 ns (10%). A comparable fit could be obtained for a single-exponential component of 6.3 ns by applying an elevated baseline.

With a 0.5-ps excitation at 298 nm in deaerated CH_3CN, a pronounced transient bleaching at 450 nm was observed (Figure 11). About 20–30% of the bleaching occurs within the laser pulse and does not recover on the time scale of the experiment (but rather in a much longer, nanosecond, time scale). The remaining part of the bleaching takes place shortly *after* the laser pulse (lifetime 30 ± 8 ps) and recovers in an intermediate time scale (lifetime 140 ± 25 ps).

Laser flash photolysis of the Ru(II)–Rh(III) dyad at 77 K with excitation at 305 nm showed bleaching of the MLCT

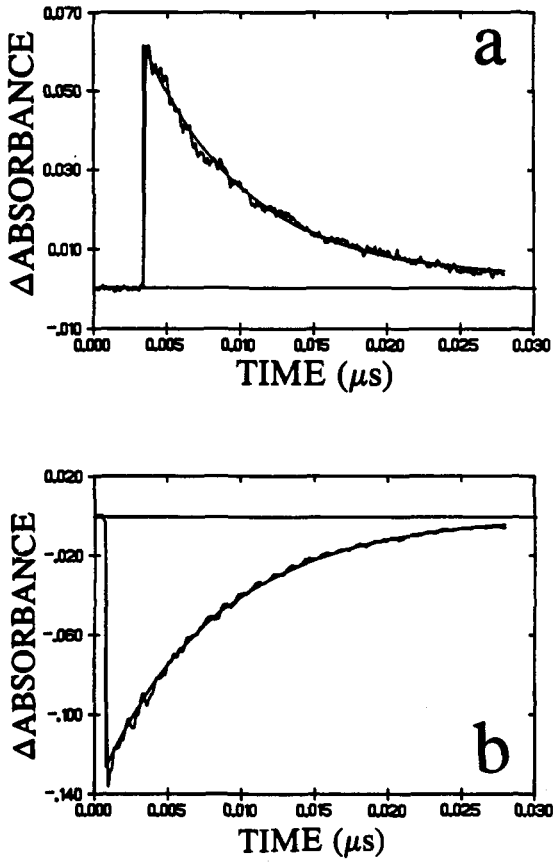

Figure 10. Kinetic profiles recorded at (a) 370 nm and (b) 450 nm following excitation of or decay of the Ru(II)–Rh(III) dyad in deoxygenated acetonitrile at 295 K with a 30-ps laser pulse at 532 nm. The computer "best fit" corresponds to a two-exponential kinetic law with lifetimes of 5.3 ns (90%) and 28 ns (10%).

absorption band of the ruthenium(II) chromophore on time scales long after the laser pulse (Figure 12). The rate constant for this bleaching process was estimated to be ca. 2×10^6 s^{-1} (Figure 12b) and was found to be independent of the concentration of the binuclear compound, at least over a narrow range. Extrapolation of the bleaching kinetic profile to the center of the exciting laser pulse indicates that about 25% of the bleaching occurs within the laser pulse. Recovery of the ground state occurs with a lifetime of 8 μs.

Discussion

Properties of Molecular Components and Energy Levels of the Dyad. The energy level diagram of the Ru(II)–Rh(III) dyad is shown in Figure 13, which includes local excited states of the molecular components as well as an intercomponent electron-transfer state. Evaluation of the intrinsic properties of the molecular components and of the energy levels of the dyad is facilitated by the fact that intercomponent interaction in this system is very weak. This is demonstrated by both the absorption spectrum (Figure 3) and the electrochemical behavior (Table 2) of the Ru(II)–Rh(III) dyad being exact superpositions of those of the Ru(II) and Rh(III) model compounds $(Ru(Me_2phen)_2(Mebpy–CH_2–CH_2–Mebpy)^{2+}$ and $Rh(Me_2bpy)_2(Mebpy–CH_2–CH_2–Mebpy)^{3+}$).

The photophysical data on the Ru(II) model compound (see Results) are typical for Ru(II) polypyridine complexes. These complexes have low-lying metal-to-ligand charge transfer excited states of "singlet" and "triplet" character.[29,30] The triplet MLCT states are populated by 100% efficient intersystem crossing in a

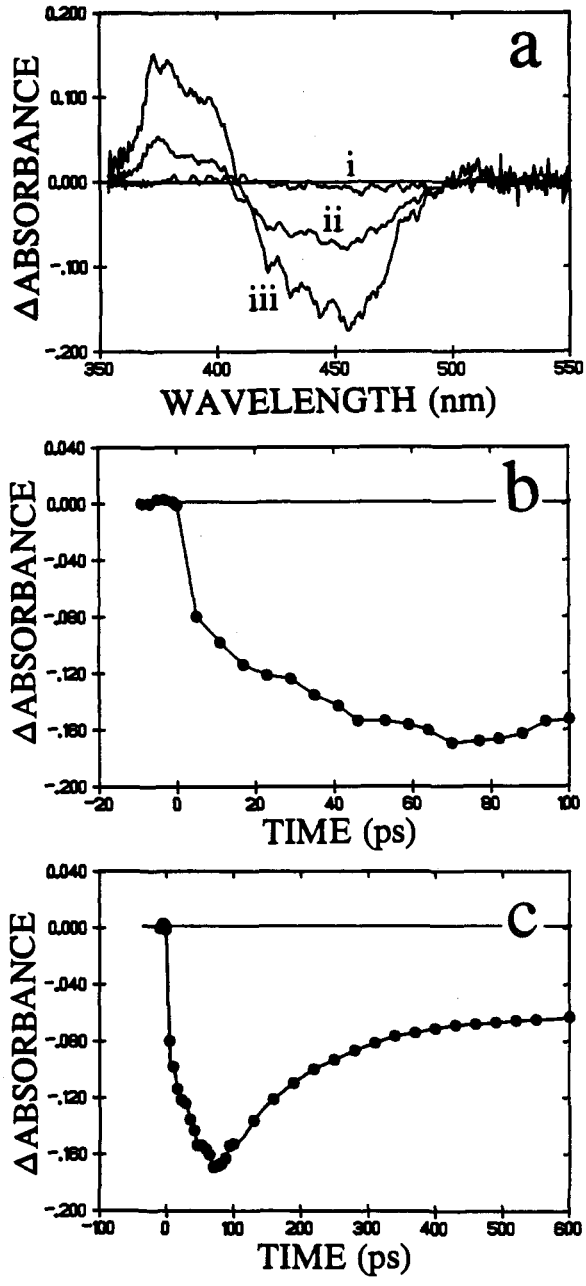

Figure 11. (a) Transient absorption spectrum recorded (i) 3 ps before, (ii) 3 ps after, and (iii) 100 ps after excitation of the Ru(II)–Rh(III) dyad in deoxygenated acetonitrile at 295 K with a 0.5-ps laser pulse at 298 nm. (b) Kinetic profile recorded at 450 nm for the above experiment showing bleaching of the ground state absorption band. (c) Kinetic profile recorded at 450 nm on a longer time scale, showing bleaching and partial recovery of the ground state absorption band. The best computed fit corresponds to lifetimes for the bleaching and recovery, respectively, of 30 and 140 ps.

sub-picosecond time scale[40] and have typical room-temperature lifetimes in the range 100–1000 ns (1–10 μs at 77 K).[30] Such MLCT states are known to have the electron localized on a single ligand, although fast interligand electron transfer causes excitation hopping.[41] In heteroleptic complexes, such hopping has been found to cause predominant fractional localization of the excited electron on the lowest energy ligand, the time scale for the interligand equilibration process being <30 ps.[42] In the present case, the MLCT state could be either of the Ru → Me_2phen or

(40) Kirk, A. D.; Hoggard, P. E.; Porter, G. B.; Rockley, M. G.; Windsor, M. W. *Chem. Phys. Lett.* **1976**, *37*, 199.
(41) Carlin, C. M.; DeArmond, M. K. *Chem. Phys. Lett.* **1982**, *89* (4), 297.
(42) Chang, Y. J.; Xu, X.; Yabe, T.; Yu, S.-C.; Anderson, D. R.; Orman, L. K.; Hopkins, J. B. J. *Phys. Chem.* **1990**, *94*, 729.

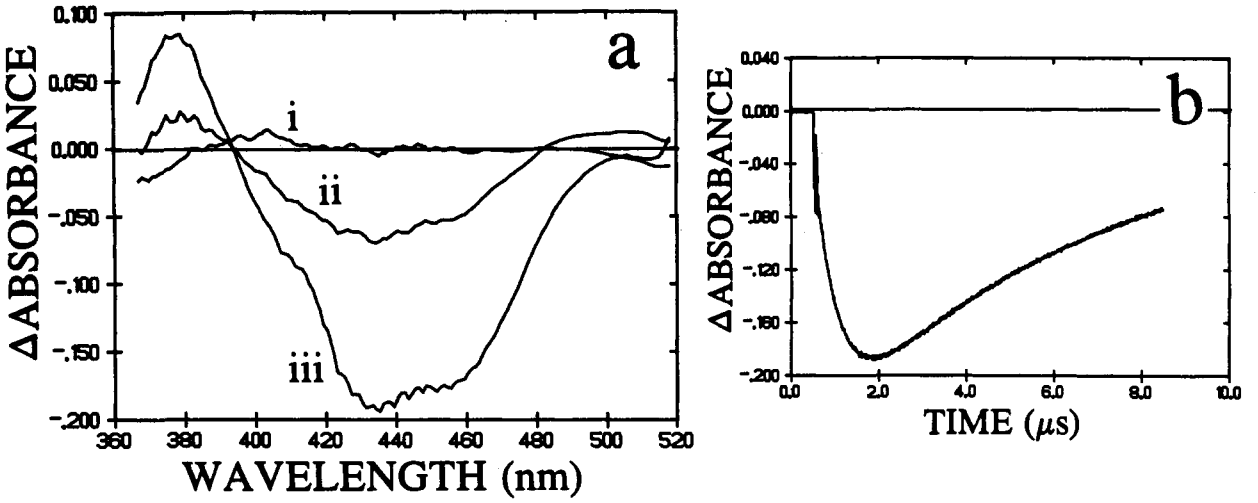

Figure 12. (a) Transient absorption spectrum recorded (i) 50 ns before, (ii) 100 ns after, and (iii) 2 μs after excitation of the Ru(II)–Rh(III) dyad in an ethanol glass at 77 K with a 10-ns laser pulse at 305 nm. (b) Kinetic profile recorded at 450 nm showing bleaching and recovery of the ground state absorption band. The best computed fit corresponds to lifetimes for the bleaching and recovery, respectively, of 520 ns and 8 μs.

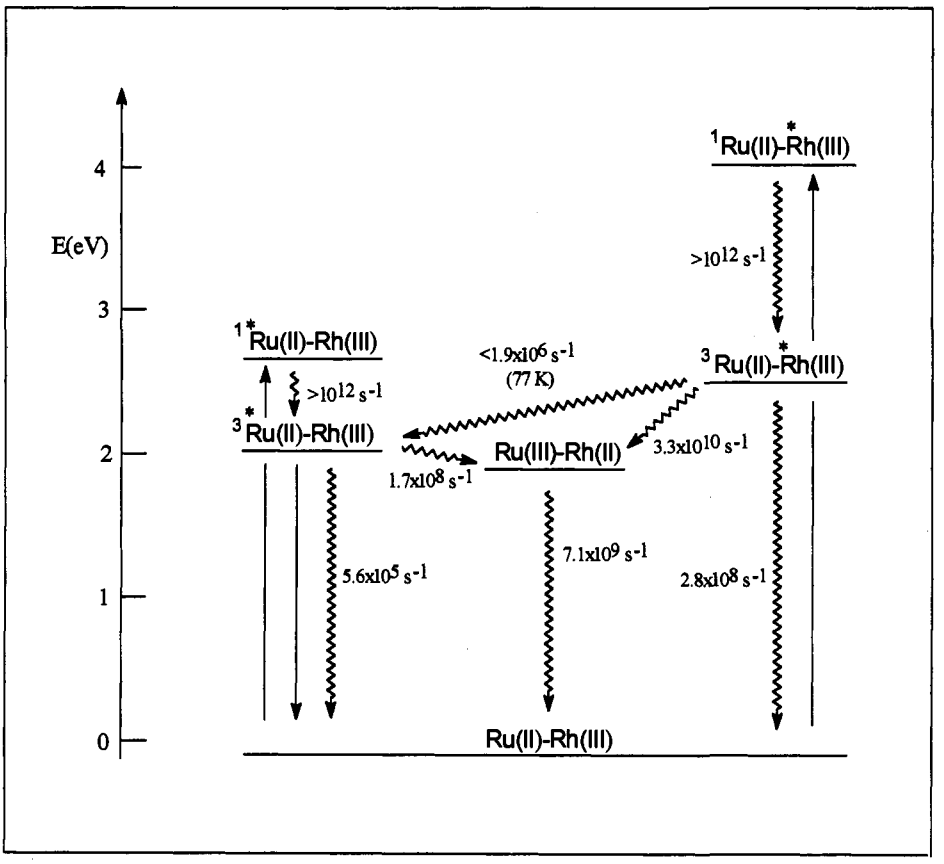

Figure 13. Energy level diagram of the Ru(II)–Rh(III) dyad. Rate constants refer to acetonitrile solutions at 295 K, unless otherwise noted.

of the Ru → Mebpy–CH_2– type. Given the similarity between the two types of ligands, however, their relative energies are difficult to predict. For the same reason, electronic spectroscopy provides no useful information regarding the localization of the excited electron. Rather, vibrational spectroscopy is the technique of choice in the form of time-resolved resonance Raman (TR^3).[22,42-45] In this respect, comparison between the TR^3 spectra of $Ru(Me_2phen)_2(Mebpy–CH_2–CH_2–bpyMe)^{2+}$, $Ru(Me_2phen)_3^{2+}$ (Figure 4 and Table 1), and $Ru(Me_2bpy)_3^{2+}$ (Figure 4 and ref 22) is instructive. In addition to some features of the ground state, the TR^3 spectra of $Ru(Me_2phen)_3^{2+}$ and $Ru(Me_2bpy)_3^{2+}$ show vibrational features which are diagnostic of Ru → Me_2-phen (e.g., weak bands at 1415 and 1303 cm^{-1}) and Ru → Me_2-bpy MLCT states (e.g., prominent bands at 1210, 1291, 1333, 1449, and 1568 cm^{-1}), respectively. The TR^3 spectrum of the $Ru(Me_2phen)_2(Mebpy–CH_2–CH_2–bpyMe)^{2+}$ model compound clearly shows features of *both* Ru → Me_2bpy and Ru → Me_2phen excitation (although the different intrinsic intensities of the two types of signals apparently give more emphasis to the former). The quantitative comparison between the spectrum of $Ru(Me_2$-$phen)_2(Mebpy–CH_2–CH_2–bpyMe)^{2+}$ and that of $Ru(Me_2bpy)_3^{2+}$ indicates that the characteristic signals of Ru → Me_2bpy excitation are weaker by a factor of 3 in the mixed-ligand compound relative

(43) McClanahan, S. F.; Dallinger, R. F.; Holler, F. J.; Kincaid, J. R. *J. Am. Chem. Soc.* **1985**, *107*, 4853.
(44) Kumar, C. V.; Barton, J. K.; Gould, I. R.; Turro, N. J.; Houten, J. V. *Inorg. Chem.* **1988**, *27*, 648.
(45) Yabe, T.; Orman, L. K.; Anderson, D. R.; Yu, S.-C.; Xu, X.; Hopkins, J. B. *J. Phys. Chem.* **1990**, *94*, 7128.

to the homoleptic one. Experiments on mixed solutions demonstrate that the spectrum of $Ru(Me_2phen)_2(Mebpy–CH_2–CH_2–bpyMe)^{2+}$ is virtually indistinguishable from that of a 1/2 mixture of $Ru(Me_2bpy)_3^{2+}$ and $Ru(Me_2phen)_3^{2+}$. Thus, it seems fair to conclude that (i) in the model compound the energies of the two types of MLCT excited states are very similar if not identical and (ii) on the time scale of the experiment (0–20 ns) interligand equilibration is established,[46] so that the excited electron resides with a quasi-statistical (33%) population on the bpy-type ligand. These conclusions can be transferred to the MLCT state of the Ru(II)–Rh(III) dyad, where the excited electron is expected to be localized with a 33% probability on the Ru(II)-coordinated moiety of the bridging ligand. The single state indicated in Figure 13 as ^{3}*Ru(II)–Rh(III) is meant to indicate the manifold of three localized MLCT triplet states in approximately statistical equilibrium distribution. Its energy is taken from the maximum of the 77 K emission spectrum (Figure 5b).

The photophysical data on the Rh(III) model compound (see Results) are typical for Rh(III) polypyridine complexes. These complexes have low-lying π–π* ligand-centered (LC) excited states of singlet and triplet character.[30,33–36] The triplet LC states are populated by 100% efficient[37] intersystem crossing on a subpicosecond time scale[47] and have typical room-temperature lifetimes in the range 1–100 ns (1–100 ms at 77 K).[30,48] At room temperature, such LC triplets can be detected by transient absorption[37] but are practically nonemitting, due to their low radiative rate constants. Since the coordinated moiety of the bridging ligand at Rh(III) is virtually identical to those of the other nonbridging ligands, a purely statistical population of bridge-localized and Me_2bpy-localized states is predicted. The single LC triplet state shown in Figure 13 as Ru(II)–^{3}*Rh(III) is meant to indicate such a statistical equilibrium mixture. The energy of this state is taken from the high-energy maximum in the 77 K emission spectrum of the Rh(III) model compound.

As usual for weakly interacting systems, the energy of the intercomponent charge-transfer state, Ru(III)–Rh(II), can be obtained from electrochemical data (Table 2) as the difference in the potentials for oxidation of Ru(II) and for reduction of Rh(III), i.e., 2.07 eV. No correction for electrostatic work terms is required in this case, as the product of the electronic charges does not change in the electron-transfer process.

A specific discussion is warranted by the problem of localization of the redox orbitals in this system. As far as oxidation of the Ru(II)-based component is concerned, there is little doubt that the process involves the metal center (changing from $(t_{2g})^6$ to $(t_{2g})^5$ electron configuration). By contrast, localization of the redox orbital involved in reduction of Rh(III) polypyridine complexes has been the subject of considerable discussion.[32,49] The reduction potentials of these complexes are close to what would be expected in terms of ligand reduction. Also, the self-exchange rate constant inferred from bimolecular quenching experiments fits better to the hypothesis of reduction at the ligand rather than at the metal[49] On the other hand, there is some more direct evidence pointing toward metal reduction; namely, the poor electrochemical reversibility and the occurrence of disproportionation reactions upon reduction are as expected for Rh(II). Localization of the added electron at the metal is also strongly indicated by the absence of intense visible absorption associated to the polypyridine radical anion in the transient spectra of the reduced forms of these complexes.[49] Taken together, these data indicate to us that, although the metal-centered and ligand-centered redox orbitals might be very close in energy, reduction at the metal is thermodynamically favored in these systems. Therefore, the reduced forms of rhodium polypyridine complexes, including the molecular component used in this dyad, can be regarded as equilibria of the type, e.g.,

$$[Rh^{II}(Me_2bpy)_3]^{2+} \rightleftarrows [Rh^{III}(Me_2bpy)_2(Me_2bpy^-)]^{2+} \quad (1)$$

with appreciable displacement toward the left.

The energy level diagram of Figure 13 indicates that various intercomponent transfer processes are thermodynamically allowed in this system, following excitation of either of the two molecular components. Making the usual assumption (for coordination compounds of this type)[40,47] that excitation of each component is followed by ultrafast intersystem crossing to the lowest triplet, the allowed processes are electron transfer from *Ru(II) to Rh(III) (eq 2), electron transfer from Ru(II) to *Rh(III) (eq 3),

$$*Ru(II)–Rh(III) \rightarrow Ru(III)–Rh(II) \qquad \Delta G° = -0.10 \text{ eV} \quad (2)$$

$$Ru(II)–*Rh(III) \rightarrow Ru(III)–Rh(II) \qquad \Delta G° = -0.70 \text{ eV} \quad (3)$$

$$Ru(III)–Rh(II) \rightarrow Ru(II)–Rh(III) \qquad \Delta G° = -2.07 \text{ eV} \quad (4)$$

$$Ru(II)–*Rh(III) \rightarrow *Ru(II)–Rh(III) \qquad \Delta G° = -0.61 \text{ eV} \quad (5)$$

back electron transfer from Rh(II) to Ru(III) (eq 4), and energy transfer from *Rh(III) to Ru(II) (eq 5). As shown in eqs 2–5, all these processes take place and can be kinetically resolved, under the appropriate experimental conditions, in this system.

Excitation of the Ru(II)-Based Molecular Component. Light in the visible region selectively excites the Ru(II)-based component of the dyad (Figure 3). In the absence of any competing intercomponent process, this molecular component should exhibit the properties of the $Ru^{II}(Me_2phen)_2(Mebpy–CH_2–CH_2–Mebpy)^{2+}$ model compound, i.e., an MLCT emission with Φ = 0.11 and τ = 1.8 μs (room temperature, degassed acetonitrile solution). Actually, in the dyad this emission has (Figure 7) a much smaller intensity ($\Phi = 7.6 \times 10^{-4}$) and faster decay ($\tau$ = 6 ns for the major component, see below). This observation clearly shows that efficient intramolecular quenching of the Ru(II)-based molecular component takes place. On the basis of the energy level diagram of Figure 13, the only available pathway for the observed quenching is photoinduced electron transfer (eq 2), followed by thermal back electron transfer (eq 4).

The experimental emission decay is a complex one (Figure 6), consisting of a major short-lived component (τ = 6 ns; ca. 85%) and a minor long-lived component ($\tau \geq 30$ ns; ca. 15%).[50] Two plausible explanations could be tentatively advanced to account for this complex decay pattern:

(i) A fast *equilibrium* between *Ru(II)–Rh(III) and Ru(III)–Rh(II) is established before back electron transfer to the ground state takes place. In such a case, the time scales of the fast and slow components would correspond to the equilibration step and the back electron transfer process, respectively, while the ratio

(46) Time-resolved resonance Raman experiments have shown that in other mixed-ligand Ru(II) complexes (e.g., containing 2,2′-bipyridine and 2,2′-bipyrimidine) interligand electron transfer takes place in less tha 30 ps.[45]

(47) In picosecond laser flash photolysis, formation of the LC triplet state of Rh(III) polypyridine complexes is complete in τ < 30 ps (Indelli, M. T.; Serpone, N. Unpublished results).

(48) Crosby, G. A.; Elfring, W. R. *J. Phys. Chem.* **1976**, *80*, 2206.

(49) Creutz, C.; Keller, A. D.; Schwartz, H. A.; Sutin, N.; Zipp, A. P. In *Mechanistic Aspects of Inorganic Reactions*; ACS Symposium Series 198; Rorabacher, D. B., Endicott, J. F., Eds.; American Chemical Society: Washington, DC, 1982; p 385 and references therein.

(50) The decay profiles can also be analyzed satisfactorily in terms of a stretched exponential decay law (O'Neil, M.; Marohn, J.; McLendon, G. *J. Phys. Chem.* **1990**, *94*, 4356) which might have more relevance for the present system. Other analytical routines can be considered, such as various statistical distributions (Harriman, A. *Pure Appl. Chem.* **1990**, *62*, 1107) or diffusive processes (Mataga, N. In *Molecular Dynamics in Restricted Geometries*; Klafter, J., Drake, J. M., Eds.; Wiley: New York, 1989; p 23), but the important point is that the observed kinetic profiles cannot be analyzed satisfactorily in terms of a single-exponential decay law.

of the two components would reflect the equilibrium distribution between the two states (and thus the ΔG° of the forward electron transfer process).

(ii) Due to the nonrigid nature of the CH_2–CH_2 bridge, various conformations of the dyad are present in solution, each with a specific rate constant for *Ru(II)-to-Rh(III) electron transfer. In such a case, the experimental trace would be a convolution of different decays, weighted according to the fractional abundance of the various conformers.

The first view was recently taken by Furue[15] to explain the nonexponential emission decay observed in a related Ru(II)–Rh(III) dyad.[51] Conformational effects, on the other hand, have often been invoked in organic dyads with flexible bridges.[52] Emission decay measurements alone cannot discriminate between the two hypotheses.[53]

The laser photolysis results are more useful in this regard. Transient absorption measurements are not as precise as the photon-counting emission decays for the purpose of detecting kinetic complications. As a matter of fact, the absorption decay can be fit equally well by a single exponential or by a double exponential (as in Figure 9, where τ = 6 and 40 ns were used, as suggested by the emission experiments). The absorption measurements, however, have the capability to discriminate between formation of the *Rh(II)–Rh(III) excited state and of the Ru(III)–Rh(II) charge-transfer state (for an example, see next section). The results show that decay of the *Ru(II)–Rh(III) excited state leads directly to the ground state, *without* any appreciable accumulation of the Ru(III)–Rh(II) charge-transfer state (Figures 8–10). This indicates that the disappearance of the Ru(III)–Rh(II) charge-transfer state by back electron transfer (eq 4) must be faster than its production (eq 2). As shown in the next section, this conclusion is directly borne out by independent experiments involving excitation of the Rh(III)-based component. Thus, the pre-equilibrium hypothesis can be definitely eliminated, and the observed emission decay must be associated with the kinetics of the forward electron transfer step (eq 2). The most plausible explanation for the biphasic kinetics involves the presence of conformers with specific rate constants, with 6 ns representing the time constant of the forward electron transfer step (eq 2) in the predominant conformer.[54]

If the difference in electron-transfer rate constants for different conformers is related to different electronic factors in the rate expression (for a discussion of the relevant kinetic factors, see below), a similar biphasic behavior should be generally expected for all the intercomponent transfer processes of this dyad (eqs 2–5). Nevertheless, since the fast kinetic component is vastly predominant and, on the other hand, any minor component would be hardly detectable in transient absorption measurements, we shall treat from now on intercomponent electron and energy transfer in this dyad as simple processes, neglecting any complication arising from conformational freedom.

Excitation of the Rh(III)-Based Molecular Component. Light in the ultraviolet region leads to substantial excitation of the Rh(III)-based molecular component (Figure 3). At 298 nm, the fraction of light absorbed by the Rh(III)-based chromophore is ca. 70%. In the absence of any intercomponent process, the behavior of this molecular component is expected to resemble that of the $Rh(Me_2bpy)_2(Mebpy–CH_2–CH_2–Mebpy)^{3+}$ model compound, where the lowest excited state has a lifetime of 4 ns (room temperature, degassed methanol).

The laser photolysis results obtained with 298-nm excitation show transient spectral changes in the visible, consisting of bleaching and recovery of the 450-nm absorbance. These transient spectral changes are made of two distinct parts (Figure 11): (i) about 20–30% of the bleaching occurs *within* the laser pulse (0.5 ps) and recovers on a very long (ns) time scale; (ii) the remaining part (70–80%) takes place *after* the laser pulse (with a lifetime of 35 ± 8 ps) and recovers over hundreds of picoseconds (lifetime of 145 ± 25 ps). Part i fits with the expectations on the basis of the amount of direct light absorption by the Ru(II)-based molecular component and of what is independently known for this type of excitation (see previous section). The second part (ii) of the transient bleaching must arise from light absorbed by the Rh(III)-based chromophore and most likely reflects formation (eq 3) and decay (eq 4) of the charge-separated state. The relative magnitudes of the two components of the transient bleaching are as expected (23% and 77%), on the basis of the partitioning of the exciting light between the Ru(II)- and Rh(III)-based molecular components and of the known molar absorptivities of the Ru(II)–Rh(III) ground state (ϵ_{450} = 20 160), the *Ru(II)–Rh(III) excited state (ϵ_{450} = 7300), and the Ru(III)–Rh(II) charge-transfer state (ϵ_{450} = 1500) at the monitoring wavelength.[55] Thus, 30 ps is the lifetime for formation of the Ru(III)–Rh(II) state, while 140 ps is the lifetime for its decay by charge recombination. This last figure justifies our failure to observe this intermediate following visible excitation of the Ru(II)-based chromophore, when the species is formed by a slow (6 ns) process and cannot accumulate to an appreciable amount.

Temperature and Medium Effects. The excitation spectrum of the residual Ru(II)-based emission in room-temperature fluid solution (Figure 7) clearly lacks the Rh(III)-based absorption features in the 280–320-nm range. This finding indicates that the thermodynamically allowed Rh(III)-to-Ru(II) energy transfer (eq 5) does not take place with appreciable efficiency under these conditions. The obvious explanation for this behavior lies in the presence of the fast electron transfer process (eq 3), which is likely to compete very effectively with energy transfer for the Rh(III)-based excited state. This places a lower limit for the timescale for the energy-transfer process (eq 5) in this system, $\tau \gg 30$ ps, at 295 K.

Interestingly, the Rh(III) absorption features are present in the excitation spectrum of the Ru(II)-based emission taken at 77 K (Figure 7), showing that Rh(III)-to-Ru(II) energy transfer takes place effectively in these experimental conditions. The process can be time-resolved by transient absorption measurements (Figure 12) where formation of the Ru(II)-based excited state is observed to occur with τ = 520 ns. The apparent switching *on* of energy transfer (eq 5) in going from room-temperature fluid solutions to 77 K glasses suggests that the competing electron-transfer process (eq 3) may become inefficient in low-temperature conditions. Support for this conclusion comes from the observation that the Ru(II)-based emission, which is strongly quenched by the other excited-state electron-transfer process (eq 2) at room temperature, is not appreciably quenched at 77 K (Figure 5b).

(51) The main difference between the dyad studied by Furue[15] and the present one lies in the presence of a CH_2–$CH(OH)$–CH_2 bridge instead of the CH_2–CH_2 one. The time scale of the emission decay is longer, with a lifetime of 50 ns for the main short-lived component.

(52) Batteas, J. D.; Harriman, A.; Kanda, A.; Mataga, N.; Nowak, A. K. *J. Am. Chem. Soc.* **1990**, *112*, 126.

(53) It could be remarked that, in order to account for the observed ratio between the amplitudes of the two exponentials, the pre-equilibrium hypothesis would require that the energy gradient between *Ru(II)–Rh(III) and Ru(III)–Rh(II) is only –0.05 eV, whereas our electrochemical estimate is –0.16 eV. Due to the poor reversibility of the Rh(III) electrochemistry, however, this argument should be taken with caution.

(54) Possible differences between the conformers may involve (i) twisting of the CH_2–CH_2 bridge (e.g., transoid vs cisoid geometry) and (ii) rotation of the bipyridine rings relative to the bridge. The fist effect would tune the rates via the through-space electron-transfer distance, while the latter one would mainly affect the rates via the through-bond electronic coupling. In the first hypothesis, the experimental result would imply that the closest distance conformer is the prevailing one, a notion which is counterintuitive on both steric and electrostatic grounds (we thank a reviewer for pointing out this aspect).

(55) Since the Rh(II) component does not absorb in the visible region (Mulazzani, Q. G.; Emmi, S.; Hoffman, M. Z.; Venturi, M. *J. Am. Chem. Soc.* **1981**, *103*, 3362), the spectrum of the Ru(III)–Rh(II) charge-transfer state at 450 nm is assumed to be the same as that of Ru(III). The spectrum of the *Ru(II)–Rh(III) excited state was assumed to be the same as that obtained for the *Ru(II) model compound by nanosecond laser flash photolysis, using the benzophenone triplet as a laser actinometer.[37]

In principle, this effect could arise from two distinct reasons: (i) substantial activation being involved in both excited-state electron-transfer processes (eqs 2 and 3) and (ii) alteration of the thermodynamics of the processes (changing from exergonic to endergonic) through the glass transition, because of prevention of solvent repolarization. These two effects are difficult to disentangle, as their common condition is $\Delta G°$(fluid solution) < $-\lambda_o$ (where λ_o is the outer-sphere reorganizational energy). Apparently, both forward electron transfer processes (eq 2 and eq 3) are in this free-energy regime (see below). The fact that solvent rigidity plays, on its own, an important role in the suppression of both excited-state electron-transfer processes (eqs 2 and 3) is demonstrated by the analogous results obtained in room-temperature rigid PMMA matrices and in 77 K glasses.[56-58]

Electron-Transfer Kinetics. The rate constants observed for the three electron-transfer processes (eqs 2–4) can be discussed in terms of standard electron-transfer theory.[59-62] Given the negligible intercomponent perturbation observed, we assume that intercomponent electronic coupling is sufficiently small that the reactions belong to the nonadiabatic regime. In a simple approximation in which the solvent modes (average frequency, ν_o) are treated classically ($h\nu_0 \ll k_BT$) and the internal vibrations are represented by a single mode of average frequency ν_i, thermally frozen, and treated quantum mechanically, the rate constant is given by

$$k_{el} = (2\pi/h)H_{AB}^2(\mathrm{FCWD}) \qquad (6)$$

where H_{AB} is the electronic coupling matrix element and the Franck–Condon weighted density of states, FCWD, is given by

$$\mathrm{FCWD} = \frac{1}{(4\pi\lambda_o k_B T)^{1/2}} e^{-S}\sum_m \frac{S^m}{m!} \times \exp\left[-\frac{(\Delta G° + \lambda_o + mh\nu_i)^2}{4\lambda_o k_B T}\right] \qquad (7)$$

In this expression, $S = \lambda_i/h\nu_i$ is the electron–phonon coupling strength (representing the degree of distortion in the high-frequency mode accompanying electron transfer), λ_i and λ_o are the inner-sphere and outer-sphere reorganizational energies, and the summation extends over the number of quanta of inner vibrational mode in the product state, m.

The three electron-transfer processes studied differ considerably in their driving force values. The rate constants are plotted in Figure 14 along with a curve of log k vs $\Delta G°$, calculated according to eqs 6 and 7. The values used in the calculation are as follows: H_{AB} = 50 cm^{-1}, λ_o = 8700 cm^{-1}, ν_i = 500 cm^{-1}, S = 2. These values are by no means unique, as equally good fits could be obtained with other sets of values as well.[63] They are, however, plausible on general grounds (see below) and can be used as a basis for discussing the rate-determining factors in this system.

The outer-sphere reorganizational energy value, λ_o, is as given by the standard two-sphere dielectric continuum model with an intercomponent (metal–metal) distance of 13.5 Å[64] and representative radii of 4.7 Å for the two metal polypyridine moieties.[65,66] The inner-sphere frequency value, ν_i, reflects the following assumptions: (i) internal reorganization is negligible in the $(t_{2g})^5/(t_{2g})^6$ Ru(III)/Ru(II) couple;[66] (ii) reduction of the Rh(III) polypyridine complexes takes place at the metal center; and (iii) internal reorganization can be significant for the $(t_{2g})^6/(t_{2g})^7$ Rh(III)/Rh(II) couple. Assumptions under points ii and iii have been discussed in a previous section. The consequence is that the relevant coordinates for inner-sphere reorganization are of the metal–ligand stretching type, for which a typical frequency of 500 cm^{-1} has been used. The S value used in the fit of Figure 14 corresponds to a λ_i value of 1000 cm^{-1}.

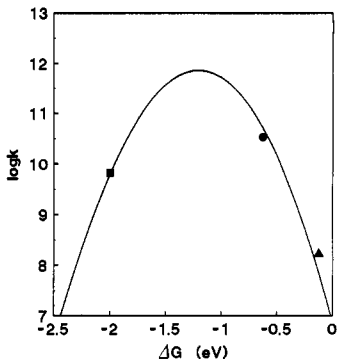

Figure 14. Plot of log k vs $\Delta G°$ for Ru(II)–Rh(III) dyad. The ▲, ●, and ■ markers indicate the k values found for the electron transfer reactions of eqs 2, 3, and 4, respectively, in CH_3CN solution. The full-line curve is calculated using eqs 6 and 7 with H_{AB} = 50 cm^{-1}, λ_o = 8700 cm^{-1}, $h\nu_i$ = 500 cm^{-1}, and S = 2.

The H_{AB} value used in Figure 14 has been chosen so as to grossly fit the three data points. It should be noted that this matrix element is expected to depend critically on the nature (distance, degree of electronic coupling, symmetry, etc.) of the donor and acceptor orbitals involved in the electron-transfer process. Thus, in principle, individual H_{AB} values should be used for each of the three data points, depending on the orbital nature of the electron-transfer process. In the forward electron transfer involving the MLCT excited state of the Ru(II)-based component (eq 1), the acceptor orbital is most likely (as discussed above) a Rh(III)-localized d orbital.[67] As to the donor orbitals, it should be recalled that time-resolved resonance Raman experiments indicate a 33% fractional population of the excited electron on the Ru(II)-bound Me–bpy–CH_2– moiety of the bridging ligand. If the H_{AB} value for hypothetical electron-transfer processes originating from the nonbridging ligands is assumed to be negligibly small,[68] the only efficient pathway would involve the π^* orbital of the Ru(II)-bound Me–bpy–CH_2– moiety of the

(56) The fact that low temperatures and rigid media do quench the electron-transfer processes but not the energy-transfer one is consistent with the notion that, in the latter process, there is no net transfer of charge between the molecular components. Thus, energy transfer requires little solvent repolarization. In a general kinetic model,[57,58] this would be represented by a much smaller λ value for energy than for electron transfer.

(57) Balzani, V.; Bolletta, F.; Scandola, F. *J. Am. Chem. Soc.* **1980**, *102*, 2152.

(58) Murtaza, Z.; Zipp, A. P.; Worl, L. A.; Graff, D.; Jones, W. E.; Bates, W. D.; Meyer, T. J. *J. Am. Chem. Soc.* **1991**, *113*, 5113.

(59) Marcus, R. A.; Sutin, N. *Biochim. Biophys. Acta* **1985**, *811*, 265.

(60) Jortner, J. *J. Chem. Phys.* **1976**, *64*, 4860.

(61) Sutin, N. *Prog. Inorg. Chem.* **1983**, *30*, 441.

(62) Miller, J. R.; Beitz, J. V.; Huddlestone, R. K. *J. Am. Chem. Soc.* **1984**, *106*, 5057.

(63) For example, a good fit would result also by the use of the following parameters: H_{AB} = 40 cm^{-1}, λ_o = 8700 cm^{-1}, ν_i = 1300 cm^{-1}, S = 0.7.

(64) Estimated from molecular models assuming a transoid geometry of the ethylenic bridge between the moieties.

(65) Following the approach of Brunschwig et al.,[66] in the two-sphere model each molecular component can be modeled by a "representative sphere", with a radius defined by

$$a = {}^1/_2(l_1 l_2 l_3)^{1/3}$$

where the l_i are the "diameters" along three mutually perpendicular axes, which can be obtained from the end-sphere radius of the component, a_{es} and the metal-to-metal distance, r:

$$l_1 = l_2 = 2a_{es}\; l_3 = a_{es} + {}^1/_2 r$$

The procedure for assigning the effective end-sphere radius a_{es} is critical. Due to the large solvent-accessible spaces between the ligands, an appropriate procedure[66] is to measure the actual volume the mononuclear complexes occupy using CPK models. For both molecular components of our Ru(II)–Rh(III) dyad, this procedure gives effective end-sphere radii of 4.3 Å (i.e., much shorter than the metal-to-polypyridine edge distances of ca. 8 Å). With a_{es} = 4.3 Å and r = 13.5 Å, a value of 4.7 Å is obtained for the radii of the representative spheres in this system.

(66) Brunschwig, B. S.; Ehrenson, S.; Sutin, N. *J. Phys. Chem.* **1986**, *90*, 3657.

bridging ligand as the donor orbital. For the other two processes observed (eqs 3 and 4) the donor and acceptor orbitals are presumably both metal-localized.[69] Thus, from this viewpoint, the process originating from the Ru(II)-based MLCT state could easily have a somewhat larger electronic factor than the other two processes. Although it would be tempting to use this argument to improve the quality of the fit, it is fair to say that the number of data points is simply insufficient for this purpose.

The important point about Figure 14 is that, regardless of the actual values of the parameters used in the fit, the main factor determining differences in observed rates is the driving force. The two photoinduced processes (eqs 2 and 3) take place on very different time scales (5 ns and 35 ps, respectively). Both are in the Marcus "normal region" ($\Delta G° > -\lambda$), but the former is only slightly exergonic whereas the latter is much more so. The relative slowness of the back electron transfer reaction (145 ps) is determined by its large driving force, which places the process in the Marcus "inverted" region ($\Delta G° < -\lambda$). The notion that electron-transfer processes belonging to the "normal" free energy region require substantial nuclear (including solvent) reorganization is in line with the experimental observation of complete suppression of the two photoinduced electron transfer processes in rigid environments.

The fact that in room-temperature fluid solution energy transfer does not compete with electron transfer no doubt arises from the smaller electronic matrix element for the former process. In this case, energy transfer is of the triplet–triplet type and is likely to be only allowed by a Dexter-type exchange mechanism. The relationships between electronic matrix elements for exchange energy transfer and related electron-transfer processes have been clearly pointed out in the classical studies of Closs and Miller.[70]

Finally, it is of some interest to compare our kinetic data with those obtained for photoinduced electron transfer in some related systems. A number of recent studies have reported rate constants for intramolecular electron-transfer quenching of excited Ru(II) (eq 2) in Ru(II)–Rh(III) polypyridine complexes.[15-17] Whereas some of these studies involve very different types of bridges, a meaningful comparison can probably be made with the work by Furue et al.[15] In such a study, aside from minor differences in the nonbridging polypyridine ligands of the two metals, the main difference is in the bridging ligand, which has a CH_2–CH(OH)–CH_2 instead of a CH_2–CH_2 link between the two Me–bpy– moieties of the bridge. The driving force for the process is estimated to be very close to that of the present work ($\Delta G° = -0.1$ eV), and yet the rate constant is 1 order of magnitude smaller than that found here.[15] The most sensible explanation of this difference is the influence of the longer (though more flexible) bridge on the electronic factor of the rate constant. A Ru(II)–Co(III) polypyridine system with the same bridging ligand as used here has been described very recently.[18] The difference in the driving force of the two intramolecular quenching processes, as well as the peculiarity of the Co(III)/Co(II) couple with respect to spin, makes any comparison of rate constants difficult. A further comparison can be made with the rate constants of intramolecular quenching in complexes of the Ru(II)–quat type (i.e., related monometallic complexes containing, besides two simple polypyridine ligands, a double bipyridine in which the pending moiety is appropriately quaternarized at the nitrogens and acts as the acceptor).[19,71] With similar $\Delta G°$ values, the rate constant values are comparable to our forward electron transfer rate constant, although the comparison is complicated in this case by the different degree of localization of the excited electron between bridging and nonbridging ligands in the two systems. As far as energy transfer (eq 5) is concerned, comparable data are unavailable, except for a report concerning energy transfer in a Ru(II)–Os(II) binuclear complex with the same double bipyridine bridge as used here.[72] A rate constant of 5.3×10^8 s^{-1} was found, but in that case a substantial contribution to the energy transfer by a Forster mechanism was suggested.

Conclusions

The Ru(II)–Rh(III) binuclear complex investigated in this work exhibits a number of interesting features. (i) In this dyad, both molecular components have long-lived excited states, which can be populated with sufficient selectivity by light absorption. (ii) A common "charge-separated" state can be reached by intercomponent electron-transfer processes originating from the two local excited states. (iii) All the intercomponent electron-transfer processes, including "charge recombination" are kinetically resolved. (iv) The electron-transfer kinetics is mainly governed by driving force, with the two "charge-separation" processes lying in the normal region and the "charge-recombination" process belonging to the inverted region. (v) Changing from fluid solutions to rigid media has the effect of switching electron transfer off and thus, apparently, energy transfer on.

The kinetic data obtained in this study can be used as a basis for the design of related triad systems featuring two-step charge separation.[73]

Acknowledgment. We are indebted to Prof. O. Bortolini for kindly measuring FAB mass spectra. J.R.S. thanks D. Bates for assistance in the Raman measurements. This work was performed with financial support from MURST, CNR (P. F. Chimica Fine), and the NSF (Grant CHE 9102657). The CFKR is supported by the Biotechnology Research Resources Program of the NIH (Grant RR00886) and by The University of Texas at Austin.

(67) As discussed above, reduction at the metal is likely to be at least slightly favored, on thermodynamic grounds, relative to reduction at the ligands. To be precise, however, both possibilities should be considered in the energy level diagram of Figure 11, in which the Ru(III)–Rh(II) state should thus be replaced with a pair of closely lying states in which the Rh(II) moiety is represented as in eq 1. In particular, it is possible that the state involving reduction at the ligand, though thermodynamically less favorable, could play a relevant *kinetic* role. This state (triply degenerate, with one third of bridging ligand character) could, in fact, have a more favorable electronic factor in intercomponent electron-transfer processes than the metal-reduced one. In the absence of an experimental test, however, such a detailed mechanistic picture should simply be regarded as a speculation.

(68) This assumption has been made in studies involving complexes of the Ru(II)–quat type (i.e., related monometallic systems where the pending moiety of the double bipyridine ligand is quaternarized at the nitrogens to act as the acceptor).[19]

(69) For the process involving the excited Rh(III)-based component (eq 3), a simple one-electron picture is probably not satisfactory. The starting Ru(II)–*Rh(III) excited state is in fact a *ligand-centered* π–π^* state while, as discussed above, formation of the Ru(III)–Rh(II) product must involve reduction at *the metal*. Thus, the reduction of the excited Rh(III)-based component in this electron-transfer reaction consists of *simultaneous* deactivation of the excited ligand and reduction of the metal center, a process which can hardly be described in simple one-electron terms.

(70) Closs, G. L.; Johnson, M. D.; Miller, J. R.; Piotrowiak, P. *J. Am. Chem. Soc.* **1989**, *111*, 3751.

(71) Yonemoto, E. H.; Riley, R. L.; Kim, Y. I.; Atherton, S. J.; Schmehl, R. H.; Mallouk, T. E. *J. Am. Chem. Soc.* **1992**, *114*, 8081.

(72) Furue, M.; Yoshidzumi, T.; Kinoshita, S.; Kushida, T.; Nozakura, S.; Kamachi, M. *Bull. Chem. Soc. Jpn.* **1991**, *64*, 1632.

(73) Indelli, M. T.; Bignozzi, C. A.; Chiorboli, C.; Scandola, F. Work in progress.